submitted to *Geophys. J. Int.*

Thermochemcial Prediction of Seismic Discontinuity Topography from Mantle Circulation Models: Supplementary information

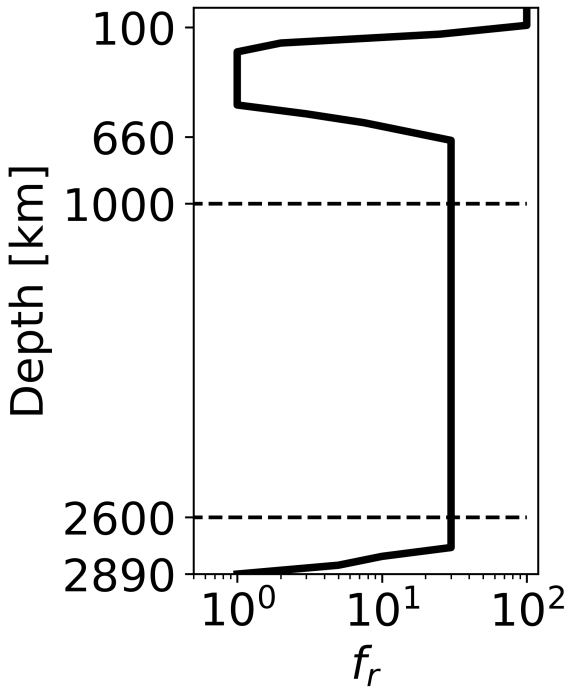

Figure S1. Variation of viscosity pre-factor with depth.

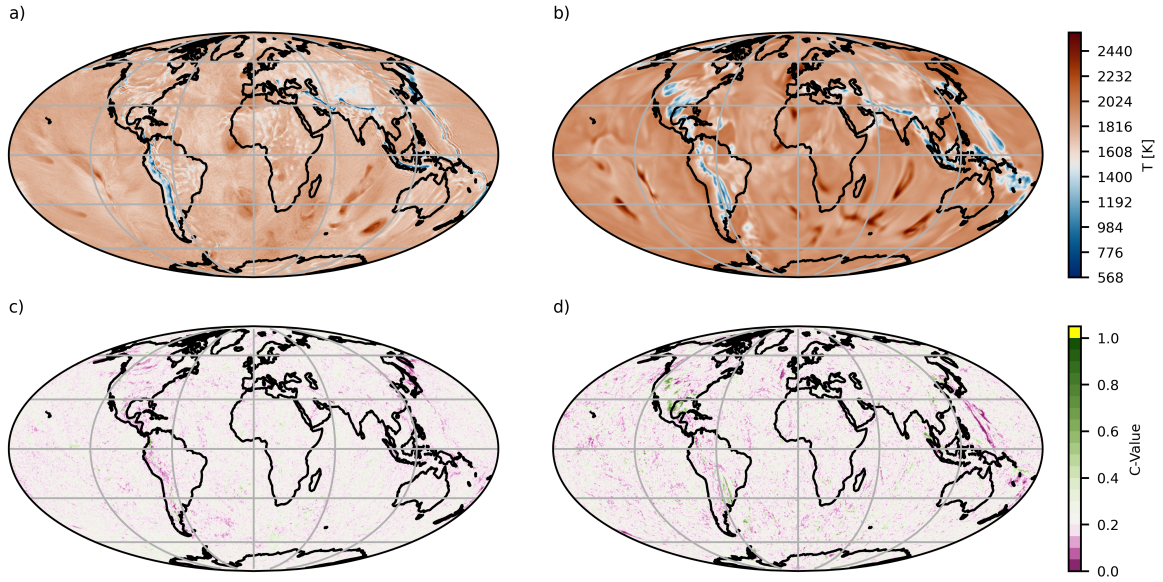

Figure S2. Thermochemical structure of simulation 'm_cc_066_u'. *a)* Thermal structure at 410 km depth *b)* C-Value structure at 410 km depth *c)* Thermal structure at 660 km depth *d)* C-Value structure at 660 km depth

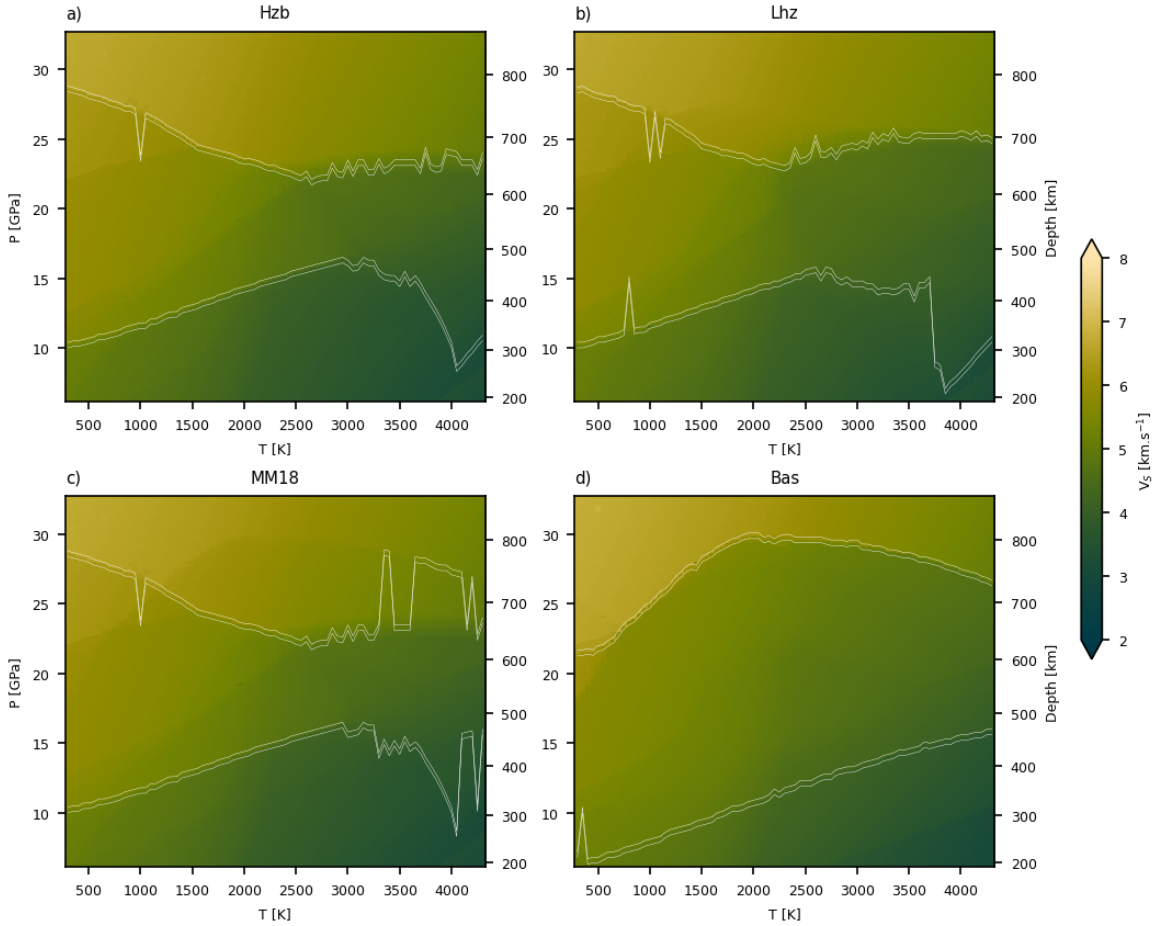

Figure S3. V_S structure of mineral physics tables for end-member compositions used in this study. *a)* Harzburgite, *b)* Lherzolite, *c)* MM18 a 'pyrolite' composition mechanical mixture of 18% Basalt and 82% Harzburgite, *d)* Basalt. V_s structure shown by color fill and the peak reflectivity pressures in the '660' and '410' regions are outlined by fine white lines 0.2 GPa above and below the picked pressure.

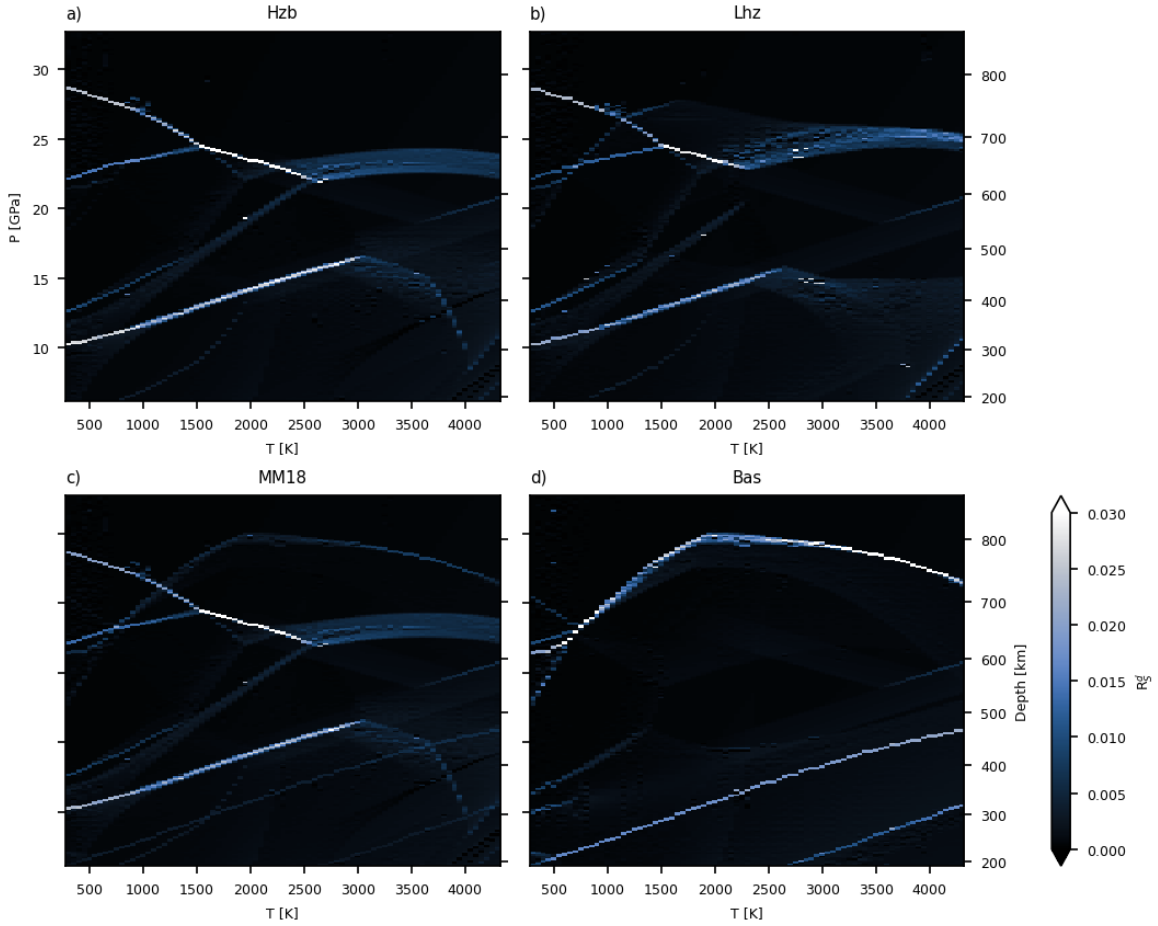

Figure S4. R_S structure of mineral physics tables for end-member compositions used in this study. *a)* Harzburgite, *b)* Lherzolite, *c)* MM18 a 'pyrolite' composition mechanical mixture of 18% Basalt and 82% Harzburgite, *d)* Basalt.

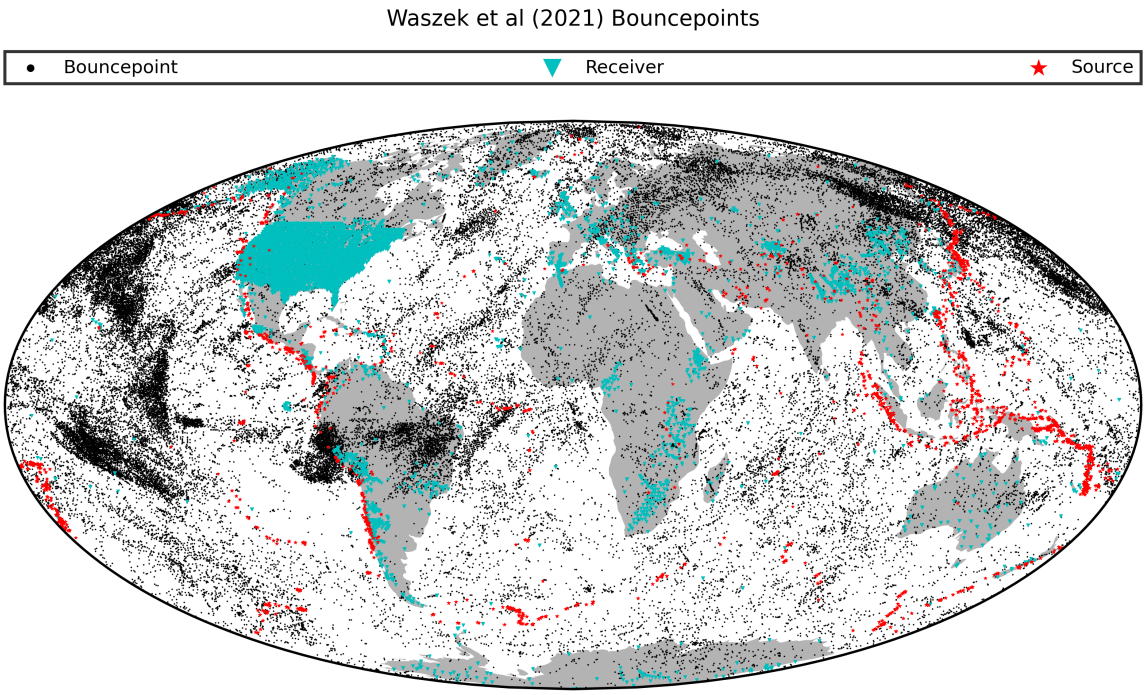

Figure S5. Distribution of seismic sources (red stars) and receivers (cyan triangles) used in Waszek et al. (2021). Bounce-points (Black dots) are then calculated as the mid-point along great circles between source-receiver pairs. Bounce-points are distributed unevenly, with clusters in the North Pacific, beneath NE Asia, Central & Eastern Europe, and Central South America.

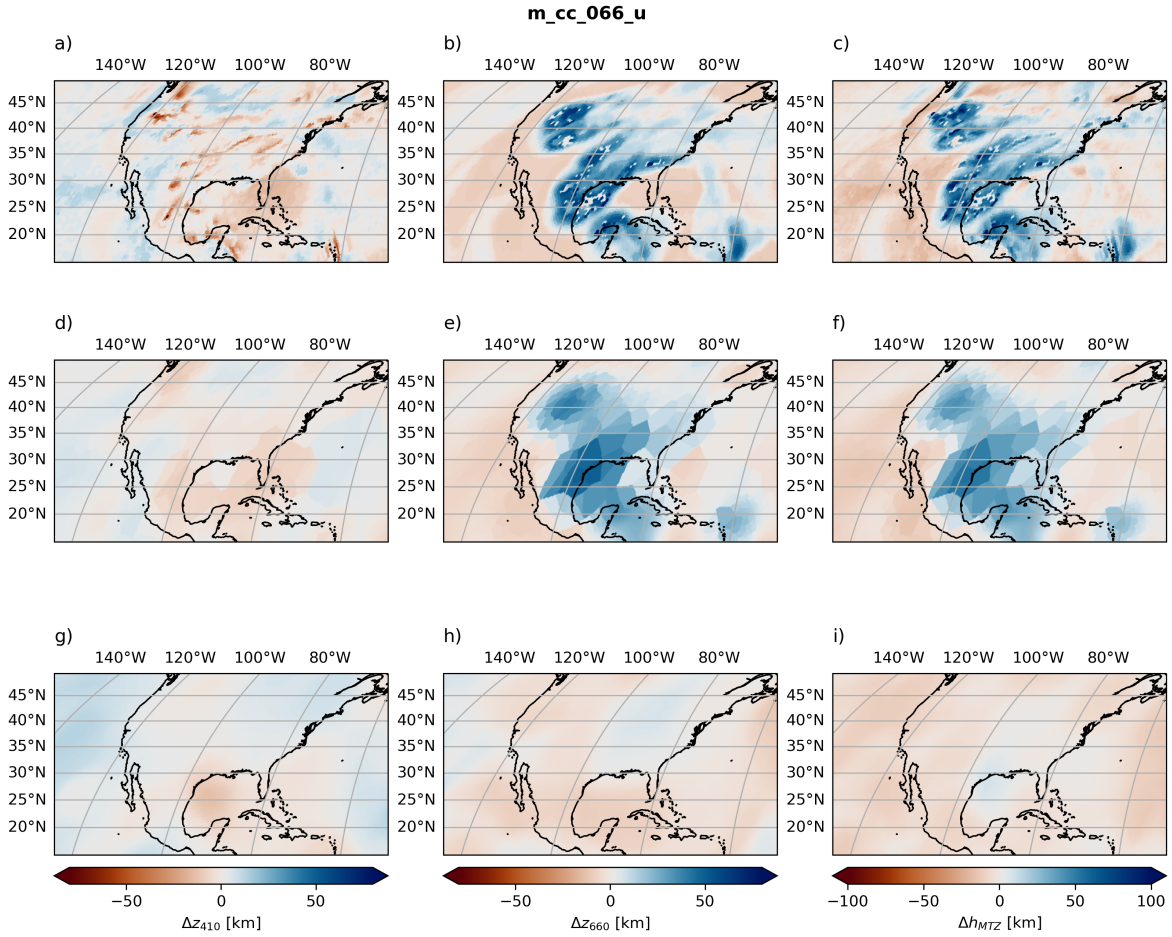

Figure S6. d410 (*a, d, g*), d660 (*b, e, h*) and MTZ thickness (*c, f, i*) topographies predicted beneath the USA and neighbouring regions from m_cc_066_u (*a–c*), predicted and filtered with a 500 km radius spherical cap (*d–f*) and the Waszek et al. (2021) model in the region (*g–i*).

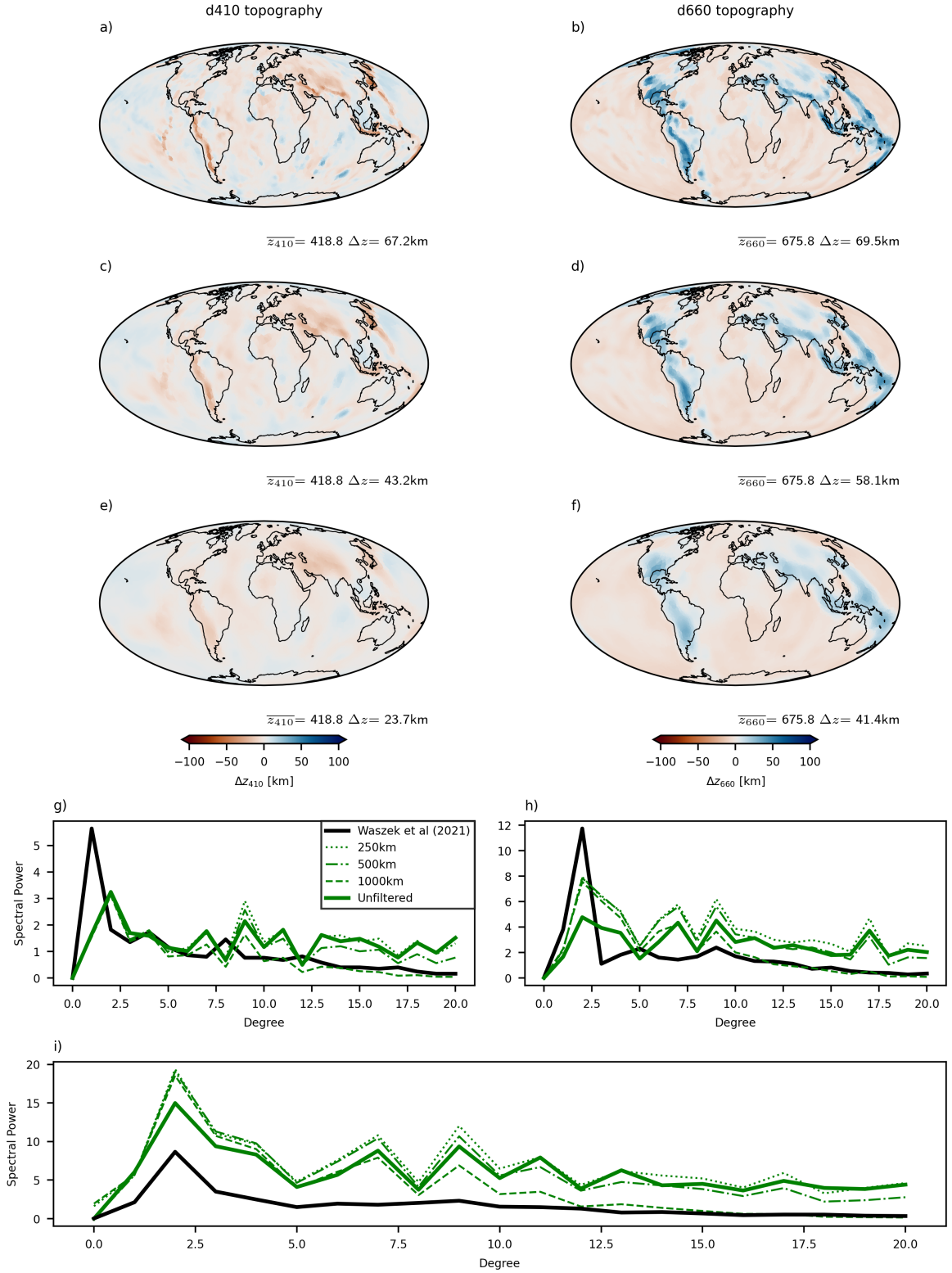

Figure S7. Variation in post-filtered topography with radius of cap used in bounce-point-spherical-cap filter. *a), c), e)* topography on 410 discontinuity with spherical cap radius 250, 500, and 1000; *km* respectively; *b), d), f)* topography on 660 discontinuity with spherical cap radius 250, 500, and 1000; *km* respectively; *g)* power spectra of 410 discontinuity with varying spherical cap radius; *h)* same as for *g*, but for 660 discontinuity. *i)* same as for g and h but for MTZ thickness

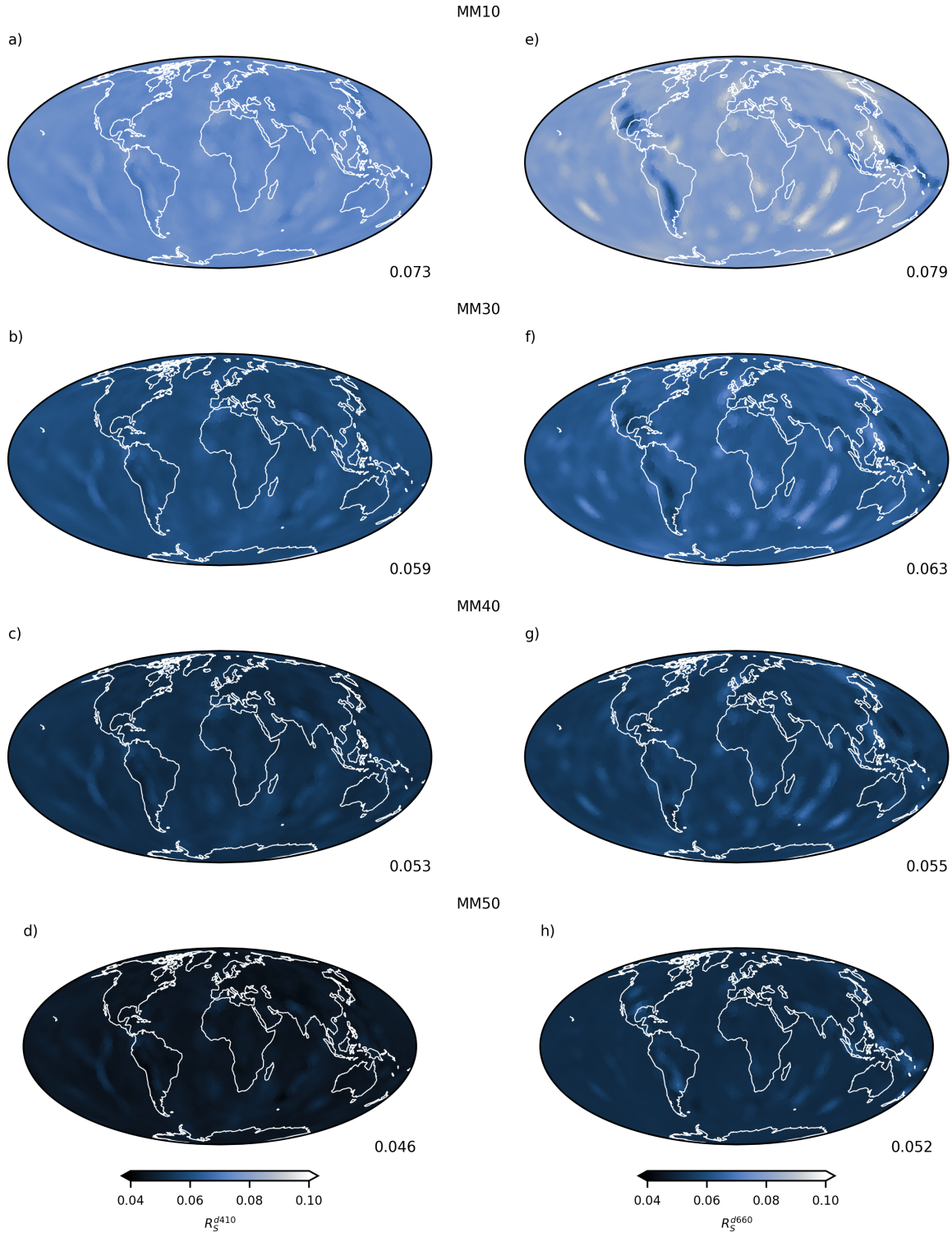

Figure S8. R_S on d410 (a–d) and d660 (e–h) for varying global mechanical mixtures MM10 (a & e), MM30 (b & f), and MM40 ((c & g) and MM50 (d and h).

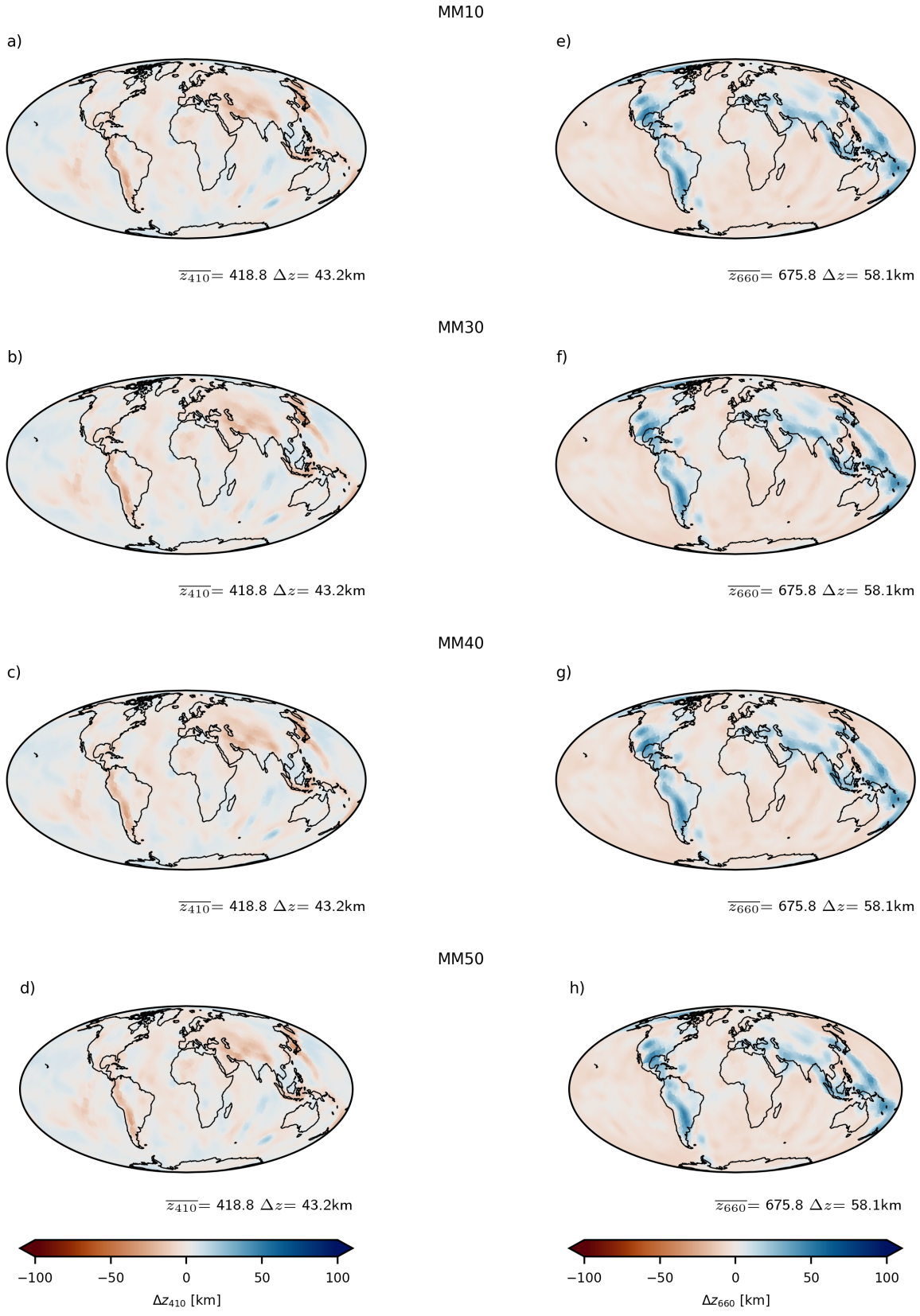

Figure S9. Filtered topography on d410 (*a*–*c*) and d660 (*e*–*g*) for varying global mechanical mixtures MM10 (*a* & *e*), MM30 (*b* & *f*), and MM40 ((*c* & *g*) and MM50 (*d* and *h*)

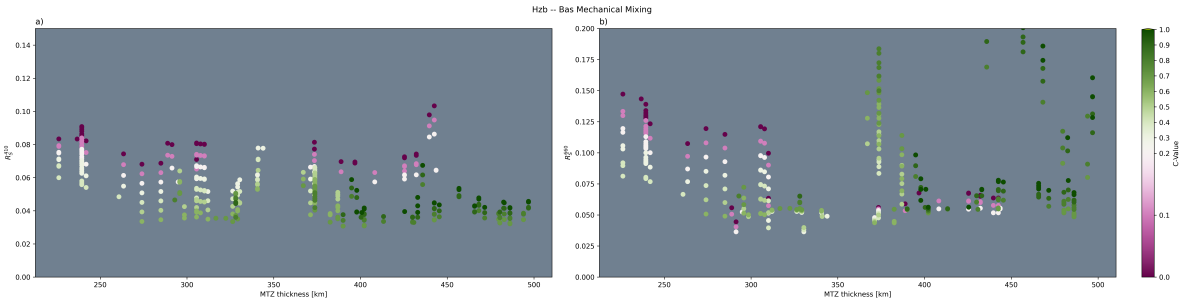

Figure S10. Relationship between R_S and MTZ thickness on *a)* d410 *b)* d660 as found from the tables used here.

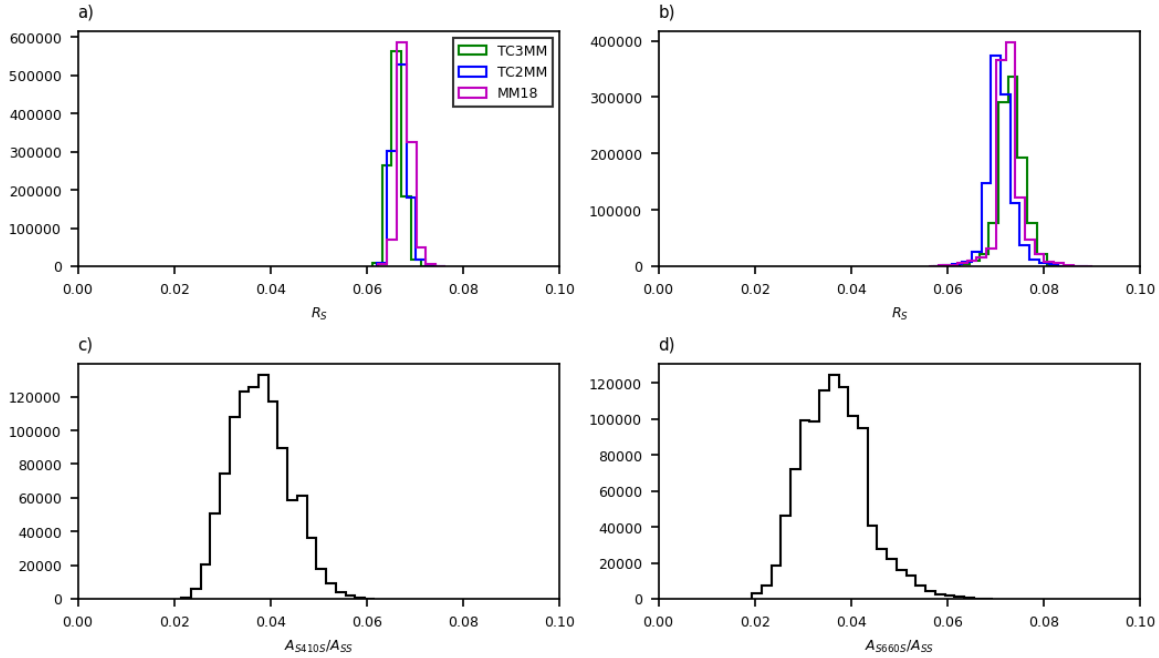

Figure S11. Histograms of *a)* R_S^{410} and *b)* R_S^{660} for the topographies predicted from the geodynamic model considered here using the local mechanical mixing assumptions and normalised SS-precursor amplitude histograms on *c)* d410 and *d)* d660 from (Waszek et al. 2021).

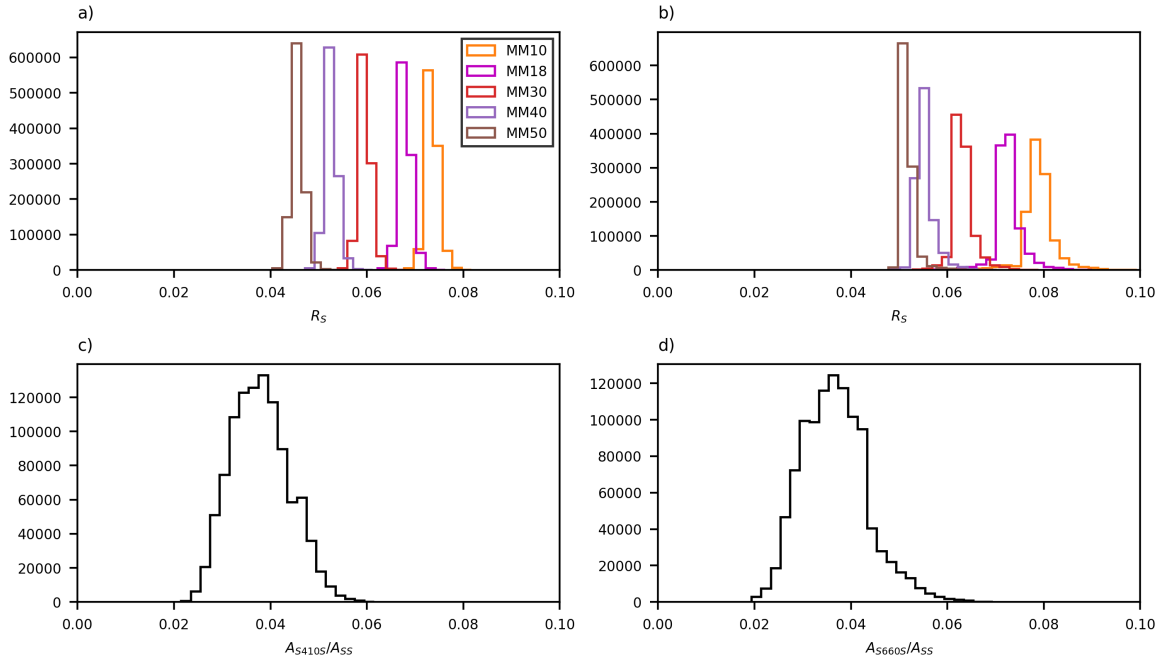

Figure S12. Histograms of *a)* R_S^{410} and *b)* R_S^{660} for the topographies predicted from the geodynamic model considered here using the different global assumed mechanical mixture compositions and normalised SS-precursor amplitude histograms on *c)* d410 and *d)* d660 from Waszek et al. (2021).

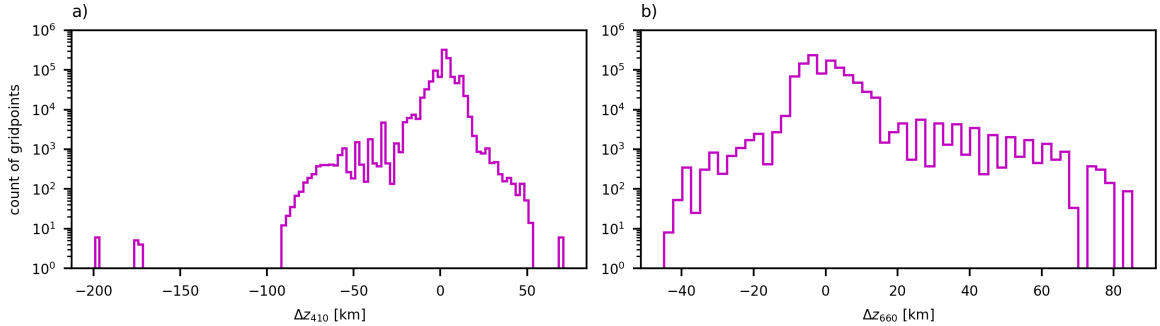

Figure S13. Histograms of *a)* d410 and *b)* d660 topography predicted from the geodynamic model 'm_cc_066_u', unfiltered using the MM18 compositional assumptions.

REFERENCES

Waszek, L., Tauzin, B., Schmerr, N. C., Ballmer, M. D., & Afonso, J. C., 2021. A poorly mixed mantle transition zone and its thermal state inferred from seismic waves, *Nature Geoscience*, **14**(12), 949–955, doi: 10.1038/s41561-021-00850-w.